Transactions, SMiRT-23
Manchester, United Kingdom - August 10-14, 2015
Division VII, Paper ID 810

Modelling the Progressive Failure of Buildings in High Winds

Peter J. Vickery[1] and Sudhan Banik[2]

[1] Principal Engineer, Applied Research Associates, Inc. Raleigh, N.C., USA
[2] Senior Engineer, Applied Research Associates, Inc. Raleigh, N.C., USA

INTRODUCTION

Wind fragility is defined as the conditional probability of failure for a given value of peak gust wind speed. The peak gust wind speed is the basic open terrain 3 second gust wind speed at 10m above grade. The widely-used method of estimating fragilities of structures and components are based on the concepts for seismic fragility analysis (e.g., Kennedy and Ravindra (1984), and by Reed and Kennedy (1994). ASME/ANS (2009)) discuss elements of the application of the methods. Park and Reich (1994) and O'Sullivan (2011) are examples of applications of these methods to wind fragility estimation. A key element in practical implementation is the use of plant design information to estimate the mean or median capacity (resistance) of the structure or component. The plant design information is generally reduced to a single value design wind speed (adjusted for load and resistance factors). Uncertainty in the mean or median capacity is generally based on published "estimates" without explicit analysis. We refer to this type of fragility analysis as Level I. Level I wind fragility analyses generally assume that all the structural elements that comprise the building envelope perform to the same level as the design of the structure. The form of the fragility functions developed using this approach is lognormal.

Here we estimate frame failure probabilities for building subjected to extreme wind loads modelling the progressive failure of components and cladding (doors, siding, roof decking) and their supporting structure (purlins and girts). The failure of these non-structural components causes changes in the buildings internal pressure, initially increasing wind loads, followed by a potential reduction of loads on primary structural elements as cladding is shed. This paper describes the modelling methodology recently used in conjunction with probabilistic risk assessments performed at some nuclear facilities in the United States. The approach builds upon the models developed for Hazus (Vickery et al, 2005), but improves the modelling through the introduction of frame failures and improved modelling of the internal pressures and the ability to model winds within a building. The model has been applied for both tornadic winds and straight-line winds. In addition to developing building fragilities, the model has been used to estimate the probabilities associated with metal siding or roof deck failing and being transported into the switchyard causing loss of offsite power (LOOP) and for estimating internal wind speeds and rain penetration into buildings.

WIND LOADS

Wind induced pressures acting on the exterior of the building are computed using:

$$p = \frac{1}{2}\rho V_z^2 GCp \qquad (1)$$

where ρ is the density of air, V_z, is the peak gust wind speed at height z, and GCp is a pressure coefficient is a coefficient. In the case of negative GCp's z is taken as the mean roof height.

The minimum values (i.e., maximum suction) of the wind load coefficients for the roof are based on those prescribed in American Society of Civil Engineers Standard 7 (ASCE 7-10); however, for low-rise

buildings the corner and edge coefficients have been increased over the values given in ASCE 7 owing to the fact that the ASCE based corner and edge loads generally understate the true magnitude of the GCp values (e.g. Vickery et al., 2011). The magnitude of the corner and edge zone pressures are similar to those prescribed in ASCE 7-10 for buildings greater than 60' tall, but the interior value of *GCp* matches that prescribed for buildings less than 60' in height.

Table 1 presents the values of the negative *GCp* values used in the fragility modelling.

Table 1. Minimum Values of Roof *GCp* Used in Fragility Modelling

ASCE Pressure Zone	GCp (Negative Pressures)
Roof Zone 3 (Corner)	-3.2
Roof Zone 2 (Edge)	-2.4
Roof Zone 1 (Field)	-1.0

GCp's for the walls and their variation with wind direction is shown in Figure 1. As indicated in Figure 1, the corner suction *GCp*'s are greater than those given in the ASCE 7 low-rise provisions but higher than those given for high-rise buildings. The mid-wall suction *GCp*'s are much less than those specified in ASCE 7. All *GCp*'s are modelled using a normally distributed error term having a coefficient of variation of 10%.

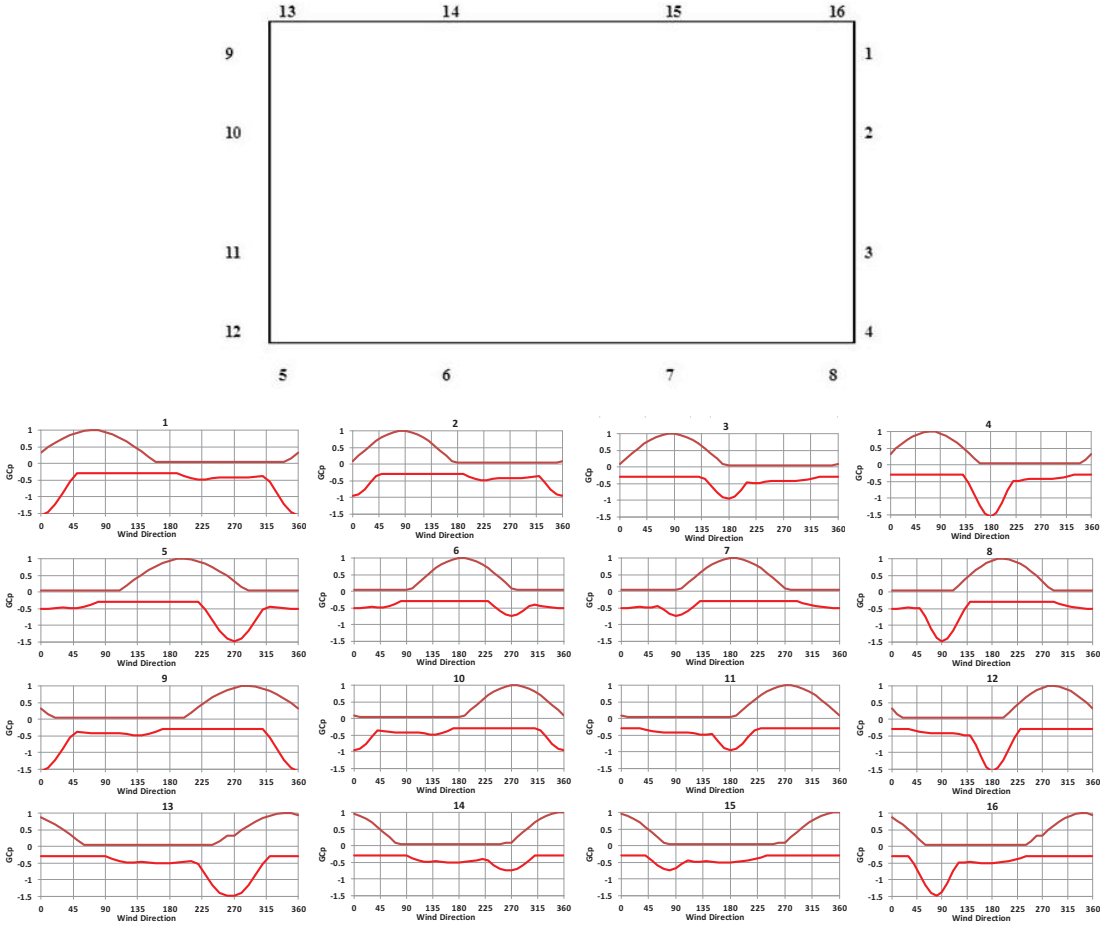

Figure 1. Wall *GCp*'s as a function of wind direction. Locations 13, 14, 15 and 16 are on the north face of the building.

Wind loads on roof and wall panels and were not reduced to account for panel area which is a slightly conservative assumption. However, in the case of the wall cladding, the effective wind area for a single connector is usually less than 10 feet so no adjustment is warranted. Similarly, in the case of the roof panels, the effective wind areas providing uplift resistance at the location of a connection are usually in the range of 10 square feet, particularly near corners where there should be more fasteners per area. A panel is considered to have failed if any one of the fasteners fails.

Wind loads acting on the roof deck elements are transferred to the purlins. These roof area loads (for purlins and beams) are reduced according to the reduction factors given in Figure 2. These factors take into account the lack of correlation of the peak pressures over large areas. The reduction factors, given in Figure 2, are based upon the *GCp*'s presented in Figure 6-11B of ASCE 7-05

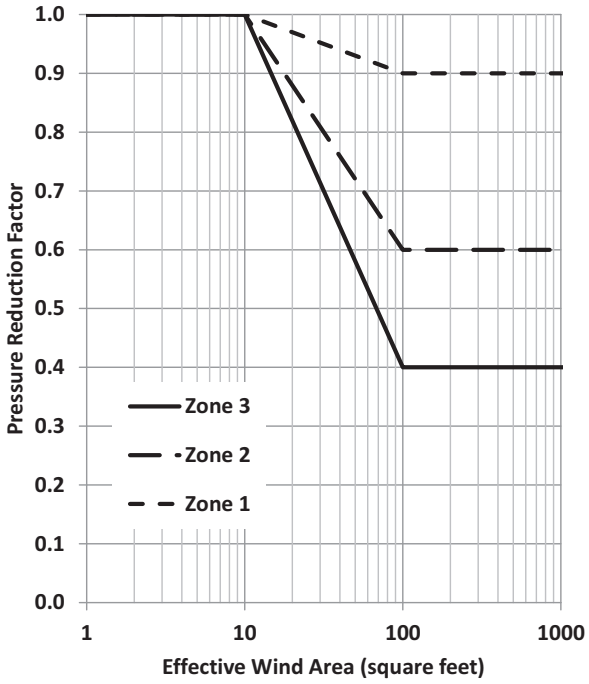

Figure 2. Pressure reduction factors used for reducing GCp values for use in computation of roof loads on purlins and roof beams

The component and cladding loads acting on walls are reduced by 10% for the computation of wind loads acting on a girt or column. This 10% reduction is less than specified in ASCE 7-10, resulting in slightly conservative maximum negative pressures. The maximum large area (>500 ft^2) positive pressures are comparable to those given in ASCE 7.

The building internal pressure is computed using information on the exterior pressures at the breaches and the continuity equation.

Flow into or out of the building at an opening is computed using

$$Q = C_D A_D \sqrt{\frac{2|p_{e_j} - p_i|}{\rho}} \tag{2}$$

where C_D is the discharge (or loss) coefficient for the opening, A_D is the area of the opening, p_e is the external pressure at opening *j*, p_i is the internal pressure and ρ is the density of the air (e.g., see Cook ,1990). Since the net flow into the building must be zero, the internal pressure is solved using:

$$\sum_{i=1}^{N} Q = \sum_{i=1}^{N} C_D A_D \sqrt{\frac{2|p_e - p_i|}{\rho}} = 0 \quad (3)$$

where *N* is the total number of openings.

Once the internal pressure is obtained, flow into or out of the building at any opening is computed using Equation 3. In all cases, a single effective opening associated with background leakage is added. The effective leakage area, A_D is computed using

$$A_D = \beta A_T \quad (4)$$

where A_T is the total area of the building envelope (taken here as the wall area and the roof area) and β is the envelope porosity. The porosity, β, is taken as 3.75×10^{-4} which is the average value for US and Canadian office buildings (Cook, 1990). The external pressure coefficient associated with background leakage is taken as -0.18. If background leakage is not modelled the failure of a single building envelope component (or components having the same external pressure) will result in no flow into the building, which is an unrealistic result. In some uses of the model it was necessary to estimate the velocity of the wind and or/volume or rainwater entering through an opening and into the building.

The internal pressure computed using Equations 1 through 3 is reduced by a factor that takes into account the lack of correlation. This reduction factor decreases as the number of openings increases.

BUILDING RESISTANCES

The following discusses the modelling of two different buildings at a nuclear power plant. The overall performance of the two buildings and their impact on the failure of various key safety related targets within the buildings is driven by the performance of the wall and roof cladding elements. The failure of purlins and girts results in additional cladding failure. In this example problem, the original construction drawings, and in some cases, design calculations were available to aid in developing the building resistance model.

In one of the buildings the roof structure consists of beams supported by columns (Building B). The roof structure of the larger building (Building A) consists of a large trusses spanning the full width of the building. The roof frame is considered to have failed if a single beam or truss fails. The wall frame is considered to have failed if any one single column has failed. A beam or column is considered to have failed if sufficient plastic moments occur to create a mechanism (i.e. 3 plastic moments in the case of a fixed end beam, one plastic moment in the case of a simply supported or cantilever beam).

Each roof deck or wall cladding element is associated with one or more girt and purlin and each girt of purlin is associated with the appropriate part of the main wind force resisting system (major beam, column or frame element).

Components that were considered in the fragility modelling include the wall cladding (fastened to girts with screws), roof deck (welded to purlins), girts and purlins, roof beams, vertical columns and roof truss (turbine building only).

Before the analysis can begin, each cladding element is associated with their support girts or purlin and each purlin or girt as associated with their supporting beams or columns. This mapping is used in the model to transfer loads from the cladding to the applicable supporting members.

Roof Decking and Wall Cladding

As indicated in Table 2 the cladding is attached by puddle welds (roof) and screws for the metal wall panels. These connections represent the failure modes associated with suction pressures (outward), either through fastener failure or panel pull-through The tensile capacity of the wall cladding fastening system was modelled using a 10% reduction in the capacity (to account for aging) and a coefficient of variation of 10%. The puddle welds were modelled assuming a safety factor of 1.5 with a coefficient of variation of 30%. Both coefficients of variation were modelled using a lognormal distribution.

In the case of wall panels loaded with positive pressures (inward acting) the cause of panel failure will not be the failure of the fasteners. In this case the panel is assumed to deflect inwards between the supporting girts and form a plastic moment. Once the moment capacity of the panel is reached the panel is assumed begin to resist the load through tension as the centre of the panel deflects inward. Failure occurs when the tensile capacity of the cladding material is reached.

Table 2. Characteristics of roof deck and wall cladding attachments for Building B.

Panel	Length (ft)	Width (ft)	Connections
Wall Cladding Panel	18	1	2 screws/panel, one on each girt
Roof Decking	Varies (spans three purlins with typical spacing about 6')	3	3 welds/purlin

Purlins and Beams

Purlins and beams are considered to have failed if a sufficient number of plastic moments form to create a mechanism. The computation of the failure load assumes the wind pressure acting on the roof panels, when transmitted to beams and purlins can be treated as a uniformly distributed load. With this assumption, the failure load for beams with various end conditions are given in Table 2. No reduction in the load carrying capacity of any roof framing member due to axial load arise from transmitting wall loads into columns is considered. Lateral torsional bucking of girts is treated in the model. The computed purlin and beam capacities were all associated with a 10% coefficient of variation which was modelled as normally distributed.

Table 3.Failure loads for various end fixities.

Beam End Conditions	Uniform Load, w, for Failure
Fixed-Fixed	$w = 16M_p/L^2$
Fixed-Pin	$w = 12M_p/L^2$
Fixed-Fixed	$w = 8M_p/L^2$

Tables 4 and 5 present the properties of each of the roof beams and purlins that were modelled for Building B. This detailed modelling of the capacity of each member is important for yielding reliable fragility estimates

Table 4 Roof Structure System – Building B

Beam #	Nominal Span ft	Section	Section	Z in^3	Width ft	Fy ksi	Mp (k-ft)
1,6,7,12,13,16,17,22,23,28,29,30	24	14WF43	W14X43	69.3	14.75	36	208
2,5,8,11,19,20,25,26	36	21WF62	W21X62	144	26	36	432
3,4,9,10,14,15	24	16B31	W16X31	54	26	36	162
18,21	18	16B31	W16X31	54	26	36	162
24,27	54	27WF102	W27X102	305	27	36	915

Table 5 Roof Purlins – Building B

Purlin #	Nominal Span ft	Section	Section	Z in^3	Width ft	Fy ksi	Mp (k-ft)
108,111,114,117,120	26	14WF30	W14X30	47.2	3	36	142
1,2,3,16,17,18,31,32,33,46,47,48,61,62,63,76,77,78,91,92,93,106,107	29.25	12B16.5	W12X16.5	20.6	6	36	61.8
16,28,32,44,48,60,76,88,92,104 (19,22,25,95,98,101)	26	12WF27	W12X27	38	6	36	114
All others	26	12B14	W12X14	14.9	6	36	44.7

TIME STEPPING FAILURE MODELS FOR BUILDINGS

The wind failure model for the building uses a simple time stepping load and resistance model to evaluate wind loads. The directionally dependent exterior pressure coefficient model is used in connection with component specific ultimate pressure capacity estimates to develop estimates of building performance as a function of the maximum peak (3 second) gust wind speed at a height of 10 m. Components of the building that are treated in the damage model include wall cladding, roof deck, girts, purlins, vertical wall framing members, roof beams (Building B) and the roof truss (Building A).

At the start of each simulation all the component resistance values are sampled as are the uncertainties in for each *GCp*. The uncertainties in *GCp* are modelled as independent. This assumption differs from that used in Hazus where the wind loading uncertainty was modelled as being fully correlated.

At the beginning of each of the time steps, the external pressure computed at the location of centroid of failed roof and wall panel is used in the estimation of the internal pressure. The initial internal pressure is updated as other panels fail. As components fail the internal pressure is re-computed and the wind loads on each element are recomputed and checked for failure. The failure of an element is recorded and used later to reduce the loads on each supporting purlin, girt, beam, etc. 1,000 simulations are performed for each target wind speed. Note the model does not currently separate aleatory and epistemic uncertainties.

The time series modelling methodology is presented in Figure 3.

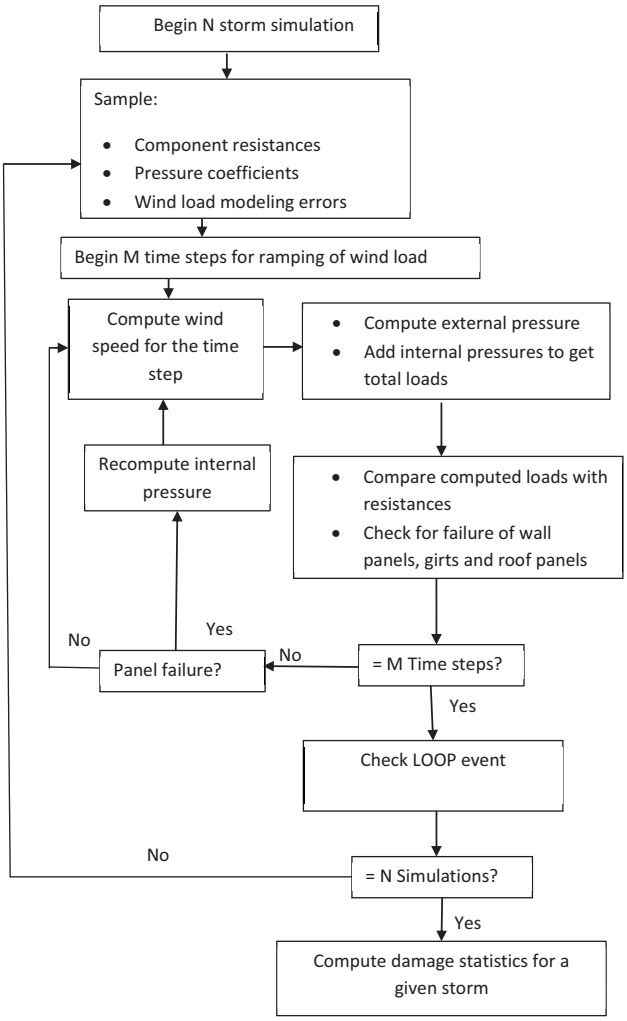

Figure 3. Progressive damage modelling methodology.

Figures 4 and 5 show the importance of the time stepping method for modelling the wind induced wall cladding failure of a building. The median wall cladding fragilities shown in Figure 4 were developed by increasing the wind speed from 80% of the maximum to 100% of the maximum in three steps. The median wall cladding fragilities shown in Figure 4 were developed by increasing the wind speed from 40% of the maximum to 100% of the maximum in 61 steps. A comparison of the two fragilities indicates that for relatively low wind speeds (i.e., less than ~120 mph) the range and rate of increase of wind speed does not make an appreciable difference to the wall clading fragilities. However, in the case of higher wind speeds the wind speed ramp rate has a significant effect on the wall cladding fragility. For example, for a wind speed of 170 mph, the three step wind speed approach significantly overestimates the wall cladding failiure probabilitities. The three step approach indicates that 100% of the cladding will fail at 170 mph, whereas the 61 step model indicates that only 15% of the cladding will have failed. The examples given in Figures 4 and 5 consider only one wind direction.

Ramping the wind speeds allows for the progressive failure of the cladding, initially causing an increase in the internal pressure resulting in inrceased loads on some panels thereby causing failure. However, as the number of failed panels increase, the internal pressure decreases (in magnitude) taking on a value near the mean of the average external pressures. This modeled reduction in the magnitude of the internal pressure is consistent with the definition of an enclosed building in ASCE 7, where after a sufficient

number of openings exist on the exterior of a building, the internal pressure reduces, taking on a value equal to that of an enclosed building. At the very high wind speeds both methods pruce the same results.Without properly ramping the wind speed the progressive failure of the cladding and the resulting changes in internal pressure cannot be properly modelled resulting in erroneous estimates of failure probabilities.

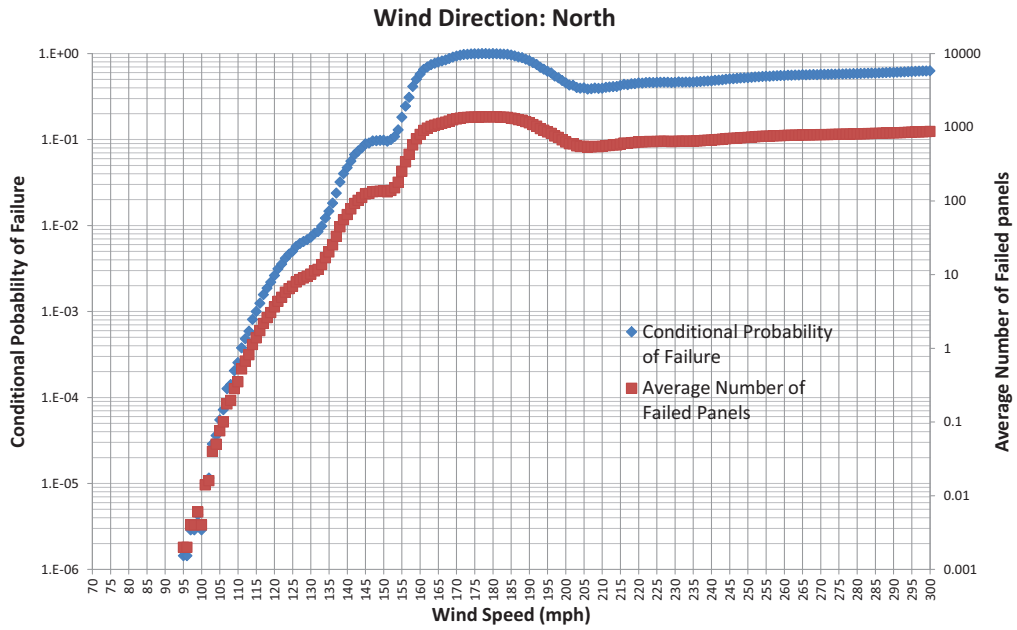

Figure 4. Wall cladding fragilities developed using a wind speed ramp function equal to 0.8, 0.9 and 1.0 times the maximum wind speed.

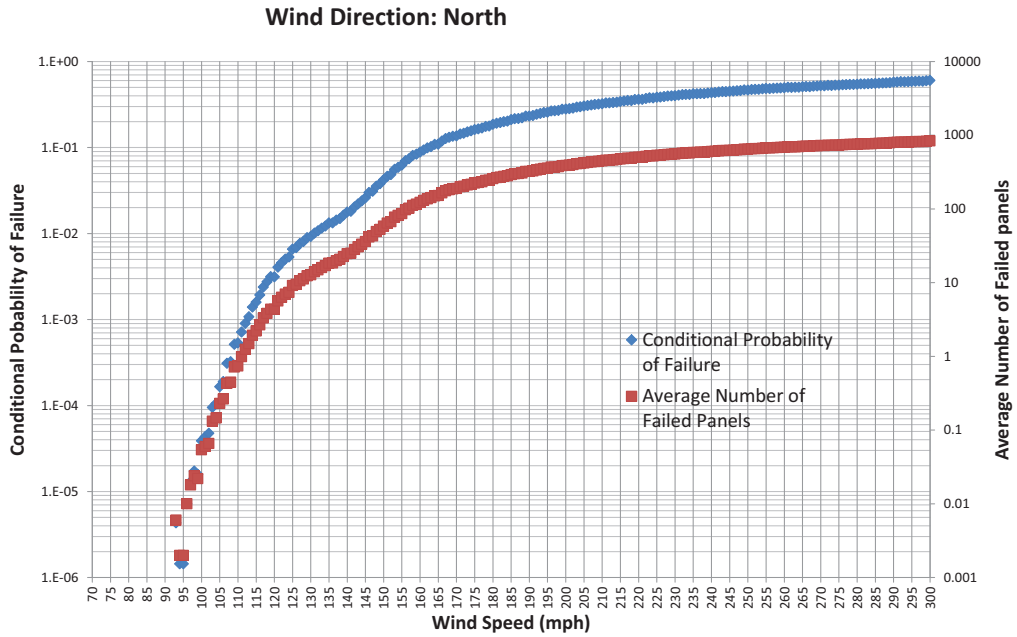

Figure 5. Wall cladding fragilities developed using a wind speed ramp function equal to 0.4, 0.41,…1.0 times the maximum wind speed.

Example Case Studies.

Figures 5 and 6 present results for two different buildings located at the same plant. Each figure shows the fragilities for the roof and wall cladding and the roof and wall frame. In the case of Building A (Figure 5) the wall cladding failures are largely caused by the failure of the screws pulling through the thin gauge sub-girts, to which the wall cladding is attached. The initial failure of the wall cladding begins at peak gust wind speeds of only 115 mph. Failure of the roof decking does not begin until wind speeds in excess of 175 mph. The frame of the building begins to fail at wind speeds of 250 mph.

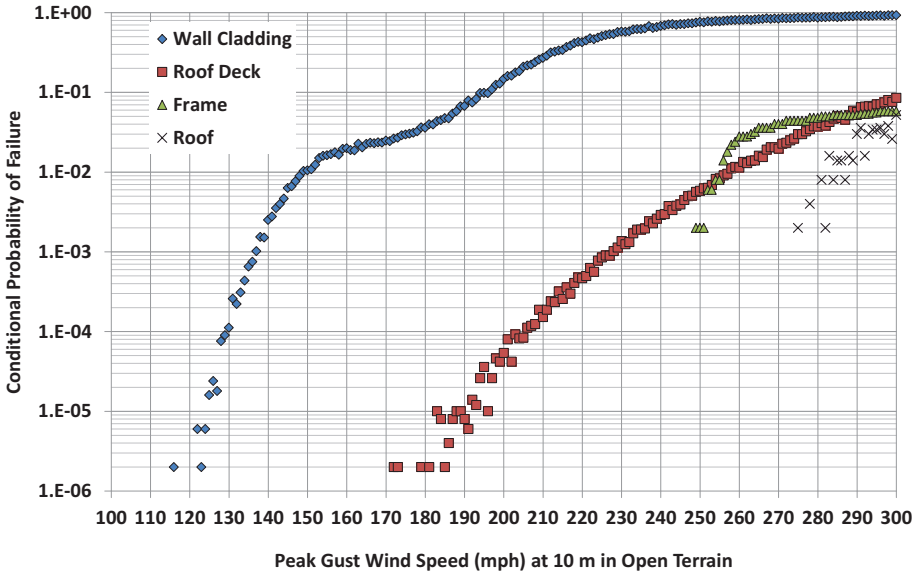

Figure 4.Wall cladding, roof deck, roof frame and wall frame fragility functions for Building A.

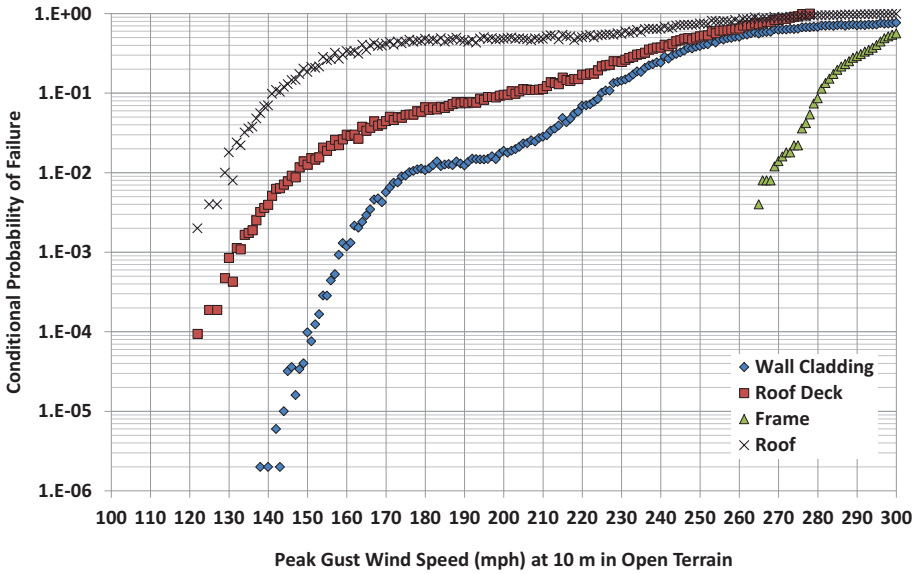

Figure 5 Wall cladding, roof deck, roof frame and wall frame fragility functions for Building B.

The roof deck on building B is attached in the same fashion is on Building B, but the much higher failure rate is caused by the failure of some long beams that have uplift capacities much less than the roof deck or

purlins. The wall cladding on building B performs better than the wall cladding on Building A because on Building B the cladding is fastened directly girts rather than through the use of light gauge sub-girts.

In both Building A and Building B, the cladding fragility function does not have the characteristic shape associated with a log-normal distribution. The two parameter lognormal distribution cannot model the effect of the internal pressure changing from an enclosed state to a partially enclosed state and then back to nearly enclosed. Similarly the effect of load reduction that occurs when components fail, and no longer load the main structural system, is hard to handle with a two parameter model.

SUMMARY

An overview of a methodology to model the progressive collapse of buildings subjected to high winds has been presented. The methodology models the variation of internal pressures as the building begins to fail. The model treats the reduction in wind loads on the main wind force resisting system as panels continue to fail. The resulting fragility curves do not fit the classic lognormal fragility models often assumed in wind fragility modelling, primarily because of the changes in the loads as the building envelope fails.

The methodology has been used to examine a number of plants in North America, including the modelling of LOOP associated with metal panels failing and being transported into the switchyard as well as estimating rain penetration into the building and wetting safety related electrical equipment.

The approach readily incorporates information on construction flaws, missing fasteners, etc., which will not be accounted for in a simple log-normal, code based fragility analysis.

REFERENCES

ASME/ANS RA-Sa-2009. “Requirements for High Wind Events AT-Power PRA”, Part 7, American Society of Mechanical Engineers, 2009.

Kennedy, R. P. and M. K. Ravindra (1984) “Seismic fragilities fir nuclear power plant risk studies”, *Nuclear Engineering and Design*, **79;** 47-68

Park, Y.J. and M. Reich. (1995)“Probabilistic Wind/Tornado/Missile Analyses for hazard and Fragility Evaluations,” Brookhaven National Laboratory, BNL-61588

Reed, J.W. and Kennedy, R.P. (1994). Methodology for Developing Seismic Fragilities, EPRI TR-103959, Electric Power Research Institute, Palo Alto, California

Vickery, P.J., J. X. Lin, P. F. Skerlj, and L. A. Twisdale Jr., (2006) “The HAZUS-MH hurricane model methodology part I: Hurricane hazard, terrain and wind load modeling”, *Natural Hazards Review,* **7**, 82-93

Vickery, P.J., P F. Skerlj, J. X. Lin, L. A. Twisdale Jr., M.A. Young and F.M. Lavelle, (2006) “The HAZUS-MH hurricane model methodology part II: Damage and loss estimation”, *Natural Hazards Review*, **7**, 94-103

Vickery, P. J., G. A. Kopp and L. A. Twisdale, Jr. (2011) “Component and cladding wind pressures on hip and gable roofs: Comparisons to the US wind loading provisions”, *13th International Conference on* Wind Engineering, Amsterdam, The Netherlands, July